THE ASTROPHYSICAL JOURNAL, 494:438–449, 1998 February 10
© 1998. The American Astronomical Society. All rights reserved. Printed in U.S.A.

A NEW METHOD FOR DIAGNOSTICS OF SOLAR MAGNETIC FIELDS AND FLOWS FROM TIME-DISTANCE ANALYSIS

MARGARITA RYUTOVA[1] AND PHILIP SCHERRER
Hansen Experimental Physics Laboratory, Stanford University, Stanford, CA 94305-4085
Received 1996 November 5; accepted 1997 September 15

ABSTRACT

We propose a new method to obtain information on plasma flows and magnetic fields below the visible solar surface using time-distance measurements. The method is based on sine and cosine transforms of propagation times measured as a function of direction. The method allows one to sort out various characteristics of the subsurface medium, the flows, magnetic fields and their nonuniformities, and is less sensitive to the measurement errors. We discuss the parity properties of various contributions to the propagation times with respect to forward and backward directions and show how these properties allow separation of the effects of magnetic field and flows, as well as separation of the horizontal components from the vertical. It is shown that the first harmonics contain information on the direction and absolute value of the velocity, while the second harmonics are sensitive to the orientation and absolute value of horizontal magnetic fields and spatial gradients of the flow velocity. We discuss the effects of discrete mesh on the accuracy of measurements of the propagation time. An advantage of the method is in its intrinsic invariance with respect to the choice of the coordinate frame. The method provides an automatic rule of assigning proper weights to every observation points. We give estimates of the accuracy of the reconstruction of the flow field over distances comparable with the scale of the convection. We also present the "magnetic" corrections to the propagation time in a vertically stratified medium.

Subject headings: convection — plasmas — Sun: magnetic fields

1. INTRODUCTION

The recent achievements in helioseismology associated with the advent of time-distance tomography have provided a wealth of information on the propagation of acoustic waves in the convective zone. This approach is based on the measurement of travel time of an acoustic wave between any point on the solar surface and a surrounding annulus. An acoustic wave propagating in the solar interior interacts with subsurface features like magnetic field, mass flows, density, and temperature perturbations. The alterations in travel time of acoustic waves due to these interactions carry important information on the subsurface structure of the solar interior. Travel-time perturbations associated with plasma flow and magnetic field under the solar surface are of particular interest.

The study of the interaction of acoustic waves with sunspots and active regions has become a special discipline in helioseismology that requires high-resolution data and adequate means for local analysis. The atmospheric manifestation of magnetic effects is complicated, for example, by the fact that strong magnetic field conglomerates absorb 30%–70% of the energy of the incoming waves (Braun, Duvall, & LaBonte 1987, 1988; Braun, LaBonte & Duvall 1990; Braun et al. 1992). Theoretical aspects of the problem include the investigation of wave propagation in strongly inhomogeneous media containing intermittent magnetic fields, plasma density and mass flows (Ryutova & Persson 1984; LaBonte & Ryutova 1993; Ryutova & Priest 1993a, 1993b; Hindman, Zweibel, & Cally 1996; Bogdan 1995 and references therein). The complicated character of the interaction of the acoustic waves with sunspot and plage regions makes the treatment of these regions quite difficult in the frame of time-distance analysis. Present analysis is applicable to regions of the quiet network.

In this paper we propose a new technique in time-distance analysis that allows study of both the effects of flows and magnetic fields. The key element of the method is that travel time is measured as a function of direction and different Fourier harmonics can be used to infer different physical parameters independently. The method allows one to sort out various characteristics of the subsurface medium including flows and magnetic fields and their nonuniformities. With increased resolution, higher harmonics could give the information about the smaller scale structures of subsurface layers. The inversion would allow one to find the depth dependence of the parameters.

The proposed technique is based on the time-distance analysis by Duvall et al. (1993, 1996). The travel times in this analysis were measured by calculating the temporal cross-correlation function between the data at some point and the data within an annulus at large distance from the point. The time measurements were performed for both forward and backward propagation, i.e., the travel times of the wave from the central point to the annulus, $\tau^{(+)}$, and back, $\tau^{(-)}$, were obtained for each of chosen annuli. Later (Duvall et al. 1998) the annuli were divided into four quadrants to measure the travel time in the north-south and east-west directions separately.

We propose a method based on the use of sin $n\theta$ and cos $n\theta$ transforms of the propagation time $\tau(\theta)$, where θ is the azimuthal angle around the annuli. We use the approximation of geometrical acoustics and assume that the magnetic effects are small. We find that the first harmonics ($n = 1$) contain information on the direction and absolute value of the horizontal flow velocity. Combinations of the second harmonics ($n = 2$) of the inward ($\tau^{(-)}$) and outward

[1] Also in Lawrence Livermore National Laboratory/Institute of Geophysics and Planetary Physics.

($\tau^{(+)}$) times are sensitive to the orientation and absolute value of horizontal magnetic fields and the spatial gradients of flow velocity. Namely, the sum of forward and backward propagating times, $\tau^{(+)} + \tau^{(-)}$, carries information on the magnetic field distribution, while the difference, $\tau^{(+)} - \tau^{(-)}$, carries information on the magnitude and orientation of shear flows. The merit of this method is in the possibility to separate the contributions of mass flows from the contribution of the magnetic fields and find the alteration of the travel time provided by flow field and magnetic field independently. Besides, this method singles out the horizontal components and is relatively less affected by the presence of vertical components of the magnetic field and mass flows.

Consider the typical geometry of time-distance analysis in helioseismology (Duvall et al. 1993) based on the measurements of the time of propagation of waves between some point A and points inside the annulus with radial width Δr on the solar surface. In Figure 1*a* the annulus in the (x, y)-plane is shown, where r is the distance between the center of annulus and some point on it and θ is an azimuthal angle that we count from west at the solar surface. The raw data contain the information about the propagation time between the point A and points in annulus. The averaged value of the propagation time could be expressed as

$$\bar{\tau} = \frac{1}{2\pi} \int_0^{2\pi} \tau(\theta) d\theta \tag{1}$$

To examine the concept of the proposed method in a simple way we consider first the continuous model where the pixels are infinitely small. The modification for the discrete measurements is straightforward but requires discussion of the errors that may appear due to the discreteness of grid points and their possible uneven distribution over the annulus. We discuss this issue in Appendix A.

The key point of our approach, as mentioned earlier, is that in addition to the average (eq. [1]) one can also take sine and cosine transforms of the propagation time

$$\bar{\tau}_c^{(n)} = \frac{1}{2\pi} \int_0^{2\pi} \tau(\theta) \cos n\theta \, d\theta \tag{2}$$

and

$$\bar{\tau}_s^{(n)} = \frac{1}{2\pi} \int_0^{2\pi} \tau(\theta) \sin n\theta \, d\theta \, . \tag{3}$$

We will discuss only averages corresponding to $n = 1, 2$ (i.e., the first and the second harmonics). Higher order harmonics carry information on the finer structures of the medium.

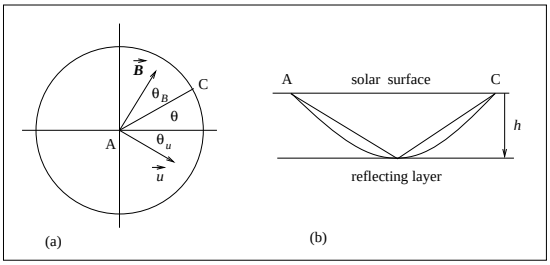

FIG. 1.—Geometry of the problem. (*a*) Annulus on the solar surface; the x-axis is parallel to the solar equator, while the y-axis is directed along the local meridian. (*b*) Ray trajectory in the model of uniform slab; AC = r.

The "directionally sensitive" information from time-distance helioseismology with MDI data was obtained by Duvall et al. (1998) by computing cross correlations between signals at a central point and four annular quadrants centered on north, south, east, and west directions. The cross correlations were averaged separately for the eastward and westward waves. The same procedure was applied to north-south propagation. The difference of forward and backward propagation times obtained in this way allowed us to find both the direction and absolute value of the flow velocity. However, the method of fixed four quadrants is not sufficient for detection of the presence of magnetic fields and/or flow nonuniformities.

The advantage of sin $n\theta$ and cos $n\theta$ transforms, besides the possibility of obtaining the information about magnetic fields, the velocity gradients, etc., is in their intrinsic invariance with respect to the choice of the coordinate frame. The method provides an automatic rule of assigning proper weights to every observation point and allows one to sort out the effects of magnetic field, flows, and their inhomogeneities in a unified manner.

The method is also preferable in some specific issues, for example, in the problem of reconstruction of the flow maps for annular distances comparable with the size of supergranular convection. The question of whether "the apparent decrease in flow with depth may be partly or entirely due to cancellation of travel-time perturbations over the annular distances of sufficient size to encounter the counterflows of neighboring supergranules" has been evoked by the referee as a question that is not addressed by either paper (i.e., the previous version of the present paper and the paper by Duvall et al. 1998). We agree with referee that "to guide the interpretation of the inversions" this question should be properly addressed. The question is indeed crucial, and not only for annular distances comparable with the size of supergranular flows, but in general for any other annular distances that become comparable to the spatial scale of any convection, granular, mezogranular, or supergranular. We address this issue in the present paper by computing the travel-time perturbations for some model of convective motions as a function of annular radii. It turned out that Fourier sin $n\theta$, cos $n\theta$ transform "kills" the largest source of errors in the reconstruction of velocity fields compared to four-quadrant method.

To illustrate the kind of information that is contained in $\bar{\tau}_{c,s}^{(1,2)}$, first we consider a simple model of acoustic wave propagation: we assume that "unperturbed" plasma parameters (i.e., parameters in the absence of flows and magnetic field) are uniform in the slab of thickness h corresponding to the lower reflection point for the acoustic wave. Then we present the corrections to the propagation time in a vertically stratified atmosphere and show that in this much more general case the alterations in the travel time still manifest the same cos $n\theta$ – sin $n\theta$ dependence on the azimuthal angle.

Throughout this paper we assume that the wavelength of acoustic waves is small compared to all other spatial scales and use the ray approximation. The results obtained for given observational data should be understood as the imaging of "large-scale" horizontal structures of magnetic field and mass flows, e.g., the variation over the scales at or larger than the radius of annuli where the measurements are taken. We also discuss a case where sound speed, flow velocity, and magnetic field weakly depend on the horizon-

tal coordinates. This allows us to find a variation of shear flows using the difference between the second harmonics of the forward and backward propagation times. Generalization of these results to the case of nonuniform unperturbed plasma parameters, arbitrary spatial dependence of flows, and magnetic field requires application of inversion routine: parity properties and angular dependences remain the same in the integral form.

At small enough u and B, such that flow velocity and Alfvén speed v_A are much less than the sound speed,

$$u, v_A \ll c_s . \tag{4}$$

The effects of flow and magnetic field enter into the propagation time $\tau(\theta)$ as small additions proportional to u/c_s and v_A^2/c_s^2, respectively. Since the conditions (4) are believed to be held for subsurface layers, one can consider the effects of flow and magnetic field separately. We will follow this line of reasoning and consider the effects of plasma flows in § 2 and the effects of magnetic field in § 3. We discuss the effects of "weak" background inhomogeneities of flow and magnetic field in § 4. In § 5 cosine and sine transforms of travel time obtained by Duvall for two sets of annuli are used to construct the maps for the distribution of horizontal magnetic field and flows at two different depths below the surface. The propagation times were measured using MDI data (T. L. Duvall 1995, private communication). Although the main purpose of this paper is to describe and discuss the new processing method and not to use it for any detailed analysis of observational data, we felt appropriate, solely for illustrative purposes, to include this section. Section 6 contains discussion of our results. Possible effects of a discrete mesh are analyzed in the Appendix A. Appendix B contains "magnetic" corrections to the propagation time in a vertically stratified atmosphere. In Appendix C we address the problem of the accuracy of reconstruction of the flow velocities for different sizes of annuli and in particular the important case when the size of annulus becomes comparable with characteristic scale of a convection.

2. THE TRAVEL TIME AND EFFECTS OF HORIZONTAL PLASMA FLOWS

2.1. *The Travel Time*

The travel time of the wave propagating with the group velocity $\boldsymbol{v}_{gr} = \partial\omega/\partial\boldsymbol{k}$ in the ray approximation is

$$\tau = \int_S \frac{1}{v_{gr}}\, ds , \tag{5}$$

where ds is an element of a ray trajectory. The dispersion relation for acoustic waves in the first approximation with respect to magnetic effects and mass flow, $\boldsymbol{u}$, has a form

$$\omega = kc_s + \boldsymbol{ku} + \frac{v_A^2}{2kc_s}\,[\boldsymbol{k} - (\boldsymbol{kb})\boldsymbol{b}]^2 , \tag{6}$$

where $\boldsymbol{b}$ is a unit vector along the magnetic field, and $k = (k_x^2 + k_y^2 + k_z^2)^{1/2}$. The group velocity is

$$\boldsymbol{v}_{gr} = \frac{\partial\omega}{\partial\boldsymbol{k}} = \frac{\boldsymbol{k}}{k}\,c_s + \boldsymbol{u} + \frac{v_A^2}{2c_s}\frac{\boldsymbol{k}}{k} - \frac{v_A^2}{c_s}\frac{\boldsymbol{b}(\boldsymbol{kb})}{k} + \frac{v_A^2}{2c_s}\frac{\boldsymbol{k}(\boldsymbol{kb})^2}{k^2} . \tag{7}$$

The absolute value of the group velocity up to the terms linear in $\boldsymbol{u}$ and quadratic in v_A is

$$v_{gr} = c_s + \boldsymbol{nu} + \frac{v_A^2}{2c_s}\,[1 - (\boldsymbol{nb})^2] , \tag{8}$$

where $\boldsymbol{n} = \boldsymbol{k}/k$.

Note that in the presence of a weak ($v_A \ll c_s$) magnetic field, in addition to the modified acoustic mode (fast-mode solution of the wave equation) that we have considered (eq. [6]), there appear two more modes, the pure Alfvén mode with

$$\omega = \boldsymbol{ku} + (\boldsymbol{kb})v_A \tag{9}$$

and a slow magnetoacoustic mode with

$$\omega = \boldsymbol{ku} + (\boldsymbol{kb})v_A - (\boldsymbol{nb})^2\,\frac{kv_A^2}{2c_s^3} . \tag{10}$$

Modes (9) and (10) have much slower group and phase velocities than the modified acoustic mode (6). These modes would correspond to much longer propagation times (c_s/v_A times longer) than the waves studied in the present frame of the time-distance analysis. Note that in the first approximation with respect to flow and magnetic field effects the dispersion relations for the Alfvén wave and slow MHD wave coincide, but they have different polarization. It might be interesting in the future to study this new domain of much longer propagation times. Although some difficulties may appear at small enough flow speed when group velocity of low-frequency modes (9) and (10) closely follows the direction of the magnetic field, so that the signal "connects" two points sitting on the same field line. Additional difficulty may consist in a strong "ballistic" damping of these modes in a nonuniform magnetic field. Still, extension of the time-distance analysis to the domain of the propagation times

$$\tau \simeq \frac{r}{v_A} \tag{11}$$

may prove to be feasible and will then provide a direct information about magnetic fields. In the first approximation with respect to magnetic and flow effects (see the conditions [4]) travel time can be written as follows:

$$\tau = \int_S \left\{\frac{1}{c_s} - \frac{\delta c_s}{c_s^2} - \frac{\boldsymbol{nu}}{c_s^2} - \frac{v_A^2}{2c_s^3}\,[1 - (\boldsymbol{nb})^2]\right\} ds . \tag{12}$$

One can see that the variation of sound speed, flows, and magnetic field have different angular dependence. Therefore, taking Fourier sine and cosine transforms (different harmonics!) of travel time one can see that the parity properties of the contribution of mass flows, magnetic effects, and variation of sound speed with respect to forward and backward propagation are different.

Additional and rich information can be obtained from the analysis of parity properties (with respect to forward and backward propagation) of the various contributions, including the spatial inhomogeneities of background parameters of medium, which can be distinguished by the Fourier sine and cosine transforms of the propagation time (eq. [12]). The Fourier transform should be performed for the forward and backward propagation times, and also for some combinations of their differences. Finally, applying an inversion procedure to the transformed times one can reconstruct the depth-dependent flow and magnetic fields below the solar surface.

2.2. *The Effects of Horizontal Flows*

As mentioned in § 1, to illustrate what kind of information is contained in $\bar{\tau}_{c,s}^{(1,2)}$, we consider here only a simple model of the acoustic wave propagation. We assume that

the "unperturbed" plasma parameters (i.e., parameters in the absence of flows and magnetic field) are uniform in the slab of thickness h corresponding to the lower reflection point for the acoustic wave. Figure 1*b* shows the geometry of the problem: acoustic waves propagating from the point A on the solar surface downward is reflected at the depth of h and propagates back to certain point C on the surface. Flow velocity is denoted by u, its direction is characterized by the angle θ_u; the magnetic field, B forms the angle θ_B with the x-axis (Fig. 1*a*). From now on we drop the bar over the propagation time symbol bearing in mind averaging is implied.

In the unperturbed state the propagation time from point A (chosen as a center of a particular annulus) to the point C on the ring of radius r is obviously

$$\tau = \tau_0 = \frac{\sqrt{r^2 + 4h^2}}{c_s} \tag{13}$$

and is the same for the waves traveling in the "forward" (from the point A to point C) and "backward" directions. In the presence of plasma flows, these times are different: the "upstream" group velocity of the acoustic wave is greater than that of "downstream."

Let the direction of flow u form an angle θ_u with the x-axis as shown in Figure 1*a*. Then from equation (12) elementary calculations (in the linear approximation) show that

$$\tau = \tau_0 - \frac{ur}{c_s^2} \cos(\theta - \theta_u) . \tag{14}$$

Integrating these expressions with $\cos\theta$ and $\sin\theta$ we obtain

$$\tau_s^{(1)} = -\frac{ur}{2c_s^2} \sin\theta_u, \; \tau_c^{(1)} = -\frac{ur}{2c_s^2} \cos\theta_u , \tag{15}$$

while $\tau_s^{(2)} = \tau_c^{(2)} = 0$.

The absolute value of the velocity can be found from the relationship

$$u = \frac{2c_s^2}{r} \sqrt{(\tau_s^{(1)})^2 + (\tau_c^{(1)})^2} , \tag{16}$$

while the direction of propagation may be determined from

$$\sin\theta_u = -\frac{\tau_s^{(1)}}{\sqrt{(\tau_s^{(1)})^2 + (\tau_c^{(1)})^2}} ,$$

$$\cos\theta_u = -\frac{\tau_c^{(1)}}{\sqrt{(\tau_s^{(1)})^2 + (\tau_c^{(1)})^2}} \tag{17}$$

or

$$u_x = \frac{2c_s^2}{r} \tau_c^{(1)} , \quad u_y = \frac{2c_s^2}{r} \tau_s^{(1)} . \tag{18}$$

Note that the presence of a uniform vertical flow does not affect equations (16) and (17). As to the forward ($\tau_{s,c}^{(1)+}$) backward ($\tau_{s,c}^{(1)-}$) propagation times, it is obvious that in the case of the uniform flow

$$\tau_{s,c}^{(1)+} = -\tau_{s,c}^{(1)-} . \tag{19}$$

Therefore, the "homogeneous" flow field may be found through the equations (16) and (18), using for $\tau_{s,c}^{(1)}$ either the transforms of forward propagation times, $\tau_{s,c}^{(1)+}$, or those of backward propagation times, $\tau_{s,c}^{(1)-}$, or the average of these times, $[\tau_{s,c}^{(1)+} + (-\tau_{s,c}^{(1)-})]/2$. For pure homogeneous flows all three results should be identical. Obviously such a situation is far from reality. The stronger the inhomogeneities are, the larger the discrepancies between the three velocity maps will be. The main discrepancies will be caused obviously by those effects that have the opposite parity properties, such as variation in sound speed and horizontal magnetic field nonuniformities (see § 5).

3. EFFECTS OF A HORIZONTAL MAGNETIC FIELD

We first present a derivation for the propagation time $\tau(\theta)$ in a case when a magnetic field is parallel to the x-axis . Then, we take into account the fact that θ_B is a finite angle and replace θ by $\theta - \theta_B$.

For a simple model of the magnetic field parallel to the x-axis the dispersion relation (6) in the first approximation with respect to magnetic effects has a form:

$$\omega = kc_s + \frac{v_A^2}{2kc_s} (k_y^2 + k_z^2) . \tag{20}$$

Using the equation for the ray trajectory (eq. [6]) yields

$$\tau = \tau_0 - \frac{\tau_0 v_A^2}{2c_s^2} \left[1 - \frac{r^2}{2(4h^2 + r^2)} \right] + \frac{\tau_0 v_A^2}{4c_s^2} \frac{r^2}{4h^2 + r^2} \cos 2(\theta - \theta_B) . \tag{21}$$

In this case, $\tau_s^{(1)} = \tau_c^{(1)} = 0$, while

$$\tau_s^{(2)} = \tau_0 \frac{v_A^2}{4c_s^2} \frac{r^2}{4h^2 + r^2} \sin 2\theta_B \tag{22}$$

and

$$\tau_c^{(2)} = \tau_0 \frac{v_A^2}{4c_s^2} \frac{r^2}{4h^2 + r^2} \cos 2\theta_B . \tag{23}$$

The magnetic field strength (actually, the inverse plasma beta) can be easily determined from the expressions (22) and (23):

$$\frac{v_A^2}{c_s^2} = 4 \frac{4h^2 + r^2}{r^2} \frac{\sqrt{(\tau_s^{(2)})^2 + (\tau_c^{(2)})^2}}{\tau_0} . \tag{24}$$

The orientation of the magnetic field can be determined from the following relations:

$$\sin 2\theta_B = \frac{\tau_s^{(2)}}{\sqrt{(\tau_s^{(2)})^2 + (\tau_c^{(2)})^2}} ,$$

$$\cos 2\theta_B = \frac{\tau_c^{(2)}}{\sqrt{(\tau_s^{(2)})^2 + (\tau_c^{(2)})^2}} \tag{25}$$

Indeed, using equations (24) and (25) we have for $B_x = B \cos\theta_B$ and $B_y = B \sin\theta_B$:

$$B_{x,y} = \left\{ \frac{8\pi\rho c_s^2 [(\tau_s^{(2)})^2 + (\tau_c^{(2)})^2]^{1/2}}{\tau_0 r^2/(4h^2 + r^2)} \right\}^{1/2} \times \left\{ 1 \pm \frac{\tau_c^{(2)}}{[(\tau_s^{(2)})^2 + (\tau_c^{(2)})^2]^{1/2}} \right\}^{1/2} . \tag{26}$$

It is important to note that forward ($\tau_{s,c}^{(2)+}$) and backward ($\tau_{s,c}^{(1)-}$) propagation times are the same

$$\tau_{s,c}^{(2)+} = \tau_{s,c}^{(2)-} . \tag{27}$$

This means that the half-sum of experimentally measured values of forward and backward propagation times, $\frac{1}{2}(\tau_{s,c}^{(2)+} + \tau_{s,c}^{(2)-})_{\rm obs}$ will determine the orientation and magnitude of magnetic field (see eq. [32]; the difference of these values carries the information about the gradients of mass flows). Thus, $\tau_{s,c}^{(2)}$ in equation (24) should be taken as

$$\tau_{s,c}^{(2)} = \tfrac{1}{2}(\tau_{s,c}^{(2)+} + \tau_{s,c}^{(2)-})_{\rm obs} \tag{28}$$

The presence of vertical component of a uniform magnetic field will not give a contribution to $\tau_s^{(2)}$ and $\tau_c^{(2)}$ (as well as, of course, to $\tau_s^{(1)}$ and $\tau_c^{(1)}$). This fact is one of the merits of the proposed approach that allows us to single out the influence of plasma flows from those of magnetic field on one hand and explore the orientation and magnitude of horizontal components independently from the vertical projection on the other.

4. EFFECTS OF BACKGROUND INHOMOGENEITIES

4.1. *Weak Inhomogeneities*

So far we were considering the simplest possible situation when the sound speed c_s, the flow velocity $\boldsymbol{u}$, and magnetic field $\boldsymbol{B}$ do not depend on coordinates over the space comparable with the radiis of annuli where the measurements are taken. Now we discuss possible modification of the earlier results in a case when c_s, $\boldsymbol{u}$, and $\boldsymbol{B}$ weakly depend on coordinates x and y. By a "weak" dependence we mean that they change insignificantly over the radius of the annulus; then the deviations from their constancy can be described by linear over x and y additions to otherwise constant c_s, $\boldsymbol{u}$, and $\boldsymbol{B}$. In a similar fashion one can take into account dependence over the vertical coordinate z, but we do not study this dependence in a present paper.

As corrections to the propagation times caused by the presence of mass flow, magnetic field, and inhomogeneity of sound speed are small, they can be taken into account separately, i.e., cross terms can be neglected.

Our initial system is that of a uniform slab of thickness h with a bottom perfectly reflecting acoustic waves. What is different now is that we consider possible linear (in x, y, z) corrections to c_s, $\boldsymbol{u}$, and $\boldsymbol{B}$; in other words, we assume that

$$c_s = c_{s0} + \boldsymbol{\sigma} \cdot \boldsymbol{r} , \tag{29}$$

$$u_\alpha = u_{0\alpha} + v_{\alpha\beta} \cdot r_\beta , \tag{30}$$

and

$$B_\alpha = B_{0\alpha} + b_{\alpha\beta} \cdot r_\beta , \tag{31}$$

where $\boldsymbol{\sigma}$ is a constant (independent of coordinates) vector and $v_{\alpha\beta}$ and $b_{\alpha\beta}$ are constant tensors.

Let us consider the possible effects of the inhomogeneity of these three physical parameters on the *sine* and *cosine* transforms of the propagation times.

Nonuniformities of c_s.—The vertical nonuniformity (dependence on z) does not break the cylindrical symmetry of the problem and does not contribute to $\tau_{s,c}^{(n)}$ ($n = 1, 2, \ldots$) at all. The horizontal nonuniformity (nonvanishing σ_x and/or σ_y) gives rise to the appearance of finite contributions to $\tau_{s,c}^{(1)}$. These contributions, obviously, will be identical for $\tau_{s,c}^{(1)+}$ and $\tau_{s,c}^{(1)-}$.

Variation of horizontal magnetic field.—The contribution of magnetic field effects to the group velocity scales as B^2 and, therefore, "magnetic" contributions to $\tau^{(n)}$ are even ($\tau^{(n)+} = \tau^{(n)-}$). The nonuniformity causes the appearance of the term of the type $B_{0x} b_{xy} y n_x^2$, $B_{0x} b_{xy} y n_y^2$ and $B_{0y} b_{yx} x n_y^2$. As y is proportional to $\sin\theta$, while n_x^2 and n_y^2 contain terms proportional to $\sin 2\theta$, $\cos 2\theta$, the propagation time will now contain terms proportional to $\sin\theta$, $\cos\theta$, and to $\sin 3\theta$, $\cos 3\theta$.

As, generally, the even effects caused by the uniform magnetic field are relatively weak, the appearance of the "magnetic" terms proportional to $\sin\theta$, $\cos\theta$, could be masked by the terms of the same structure appearing from the horizontal nonuniformity of the sound speed.

Variation of horizontal velocity.—The presence of the terms linear in x and y gives rise to a contribution to $\tau_{s,c}^{(2)}$ (this particular case is considered in the next section). The change of the sign of $\boldsymbol{u}$ (i.e., of both $u_{0\alpha}$ and $v_{\alpha\beta}$) is equivalent to mutual replacement of the emission source and detection points. On the other hand, the change of sign in velocity changes the sign of $\tau_{s,c}^{(2)}$. Therefore, we conclude that

$$\tau_{s,c}^{(2)+} = -\tau_{s,c}^{(2)-} . \tag{32}$$

We use this relationship below for finding the spatial distribution of mass flows through the observed propagation times.

4.2. *The Propagation Time in the Presence of Linear Variations of the Horizontal Flow Velocity*

We use the model described by equation (30). Denoting the variable part of the velocity vector by $\Delta\boldsymbol{u}$, we can write

$$\Delta u_x = u_{xx} x + u_{xy} y , \tag{33}$$

and

$$\Delta u_y = u_{yx} x + u_{yy} y . \tag{34}$$

The horizontal component of the group velocity in the case shown in Figure 1, for the ray propagating in the direction forming an angle θ with x-axis, is

$$\frac{c_s r}{\sqrt{r^2 + 4h^2}} + \Delta u_x \cos\theta + \Delta u_y \sin\theta , \tag{35}$$

or

$$\frac{c_s r}{\sqrt{r^2 + 4h^2}} + \rho\left(\frac{u_{xx} - u_{yy}}{2} \cos 2\theta + \frac{u_{xy} + u_{yx}}{2} \sin 2\theta\right), \tag{36}$$

where ρ is a polar radius, $x = \rho\cos\theta$, and $y = \rho\sin\theta$.

The propagation time up to the terms linear in $u_{\alpha\beta}$, is then (see eq. [14]),

$$\tau = \tau_0 - \frac{ur}{c_s^2}\cos\theta - \frac{1}{c_s^2} \times \left(\frac{u_{xx} - u_{yy}}{2} \cos 2\theta + \frac{u_{xy} + u_{yx}}{2} \sin 2\theta\right) \int_0^r \rho\, d\rho \tag{37}$$

or

$$\tau = \tau_0 - \frac{ur}{c_s^2}\cos\theta - \frac{r^2}{2c_s^2} \times \left(\frac{u_{xx} - u_{yy}}{2} \cos 2\theta + \frac{u_{xy} + u_{yx}}{2} \sin 2\theta\right). \tag{38}$$

The first harmonics give, obviously, the expressions for the horizontal components of uniform flow, while second harmonics include the effects of possible shear flows in the

horizontal plane:

$$\tau_s^{(2)} = -\frac{u_{xy} + u_{yx}}{8c_s^2} r^2 \quad (39)$$

$$\tau_c^{(2)} = -\frac{u_{xx} - u_{yy}}{8c_s^2} r^2 . \quad (40)$$

5. USING THE FORWARD-BACKWARD INFORMATION

5.1. *Symmetry Properties*

We summarize here the symmetry properties of various contributions to the propagation time and use our results to find the general pattern of magnetic field and flow distribution at two different layers using the observational data. The symmetry properties are shown in Table 1, which characterizes, in particular, parity properties of the forward-backward propagation times (when speaking on the propagation times in this section we mean their sine and cosine transforms). As mentioned earlier, the knowledge of these parity properties gives an additional opportunity in splitting of various effects.

In particular, if we take a half-sum of experimentally measured $\tau_{s,c}^{(2)+}$ and $\tau_{s,c}^{(2)-}$, we obtain the quantity that eliminates the contribution of the flow nonuniformity and is, thereby, directly related to the magnetic field strength by the equations (24)–(28). On the contrary, by constructing the quantity $\frac{1}{2}(\tau_{s,c}^{(2)+} - \tau_{s,c}^{(2)-})$ one can characterize the flow nonuniformities. Thus, when computing, for example $u_{xy} + u_{yx}$, we use the expression (39) in the form

$$\frac{\partial u_x}{\partial y} + \frac{\partial u_y}{\partial x} = -\frac{4c_s^2}{r^2} (\tau_s^{(2)+} - \tau_s^{(2)-}) . \quad (41)$$

As earlier, we mean here linear in x and y variation of background parameters. The presence of quadratic terms, will, obviously, give finite contributions to $\tau_{s,c}^{(2)}$, etc. Note that although the *variation* in the horizontal magnetic fields contribute to the first harmonics (last row in the Table 1), the alteration in travel time would be completely masked by the effects of a uniform mass flows (second row in the Table 1) and may be ignored in the frame of a present approximation.

5.2. *Example of the Reconstruction of Flow and Magnetic Fields Using MDI-SOHO Data*

We use here results of travel-times measurement and their sine and cosine transforms obtained by T. L. Duvall (1995, private communication). As a test of this method we analyzed a sample of data from the Michelson Doppler Imager (MDI) of the solar oscillations investigation on *SOHO*. The data were taken from the 8 hr observation of line-of-sight velocity in the MDI high-resolution field on 1996 January 27. The magnetogram of the studied region is shown in Figure 2*a* (Plate 10; magnetic field is shown in blue). The travel times have been measured for sets of ray paths on a grid of 30 × 40 points on the observed area of 175 × 130 Mm. The sine and cosine transforms have been made for two sets of short distance ray paths. Each set contains the data averaged over the three sets of annuli with the radial distance ranges of $\Delta = 0.^\circ225$–$0.^\circ625$ and $\Delta = 0.^\circ625$–$1.^\circ025$. The average over wider annuli for the case of eight directions compared for four quadrants used by Duvall et al. (1998) is required in order to maintain a usual noise level. For the reconstructed flow and magnetic fields the mean depths drop at $h_1 \simeq 1.2$ Mm and $h_2 \simeq 2.8$ Mm below the solar surface. Thus, to the first set of measured travel times and their sine and cosine transforms we prescribe the mean depth $h = 1.2$ Mm and mean annulus radius $r = 5.2$ Mm, respectively, for the second set of measured travel times we have $h = 2.8$ Mm and $r = 10$ Mm.

Figure 2*b* shows a pattern of the reconstructed magnetic field, more precisely, v_A^2/c_s^2 at the depth $h = 1.2$ Mm (blue color). One can see a strong correlation between the measured magnetic field on the solar surface and underlying horizontal field below it. The much larger scale of reconstructed local elements compared to elements on magnetogram is consistent with both the ray approximation (which does not allow one to resolve the scale less than the ray path) and the observational data that also are restricted by the size of annuli.

Figures 3*a* and 3*b* show the computed velocity field for the depths of 1.2 Mm and 2.8 Mm below the surface. The maps clearly show the supergranular pattern in the flow field. The velocity fields shown in Figures 3*a* and 3*b* are obtained from the cosine and sine transforms of the forward propagation times. As mentioned earlier (see second row in Table 1) in the absence of local inhomogeneities the velocity field reconstructed from the measurements of backward propagation times and forward propagation times should be the same. Obviously, presence of the local inhomogeneities of medium violates the exact relationship (32) and causes the discrepancies in the maps obtained from $\tau_{s,c}^{(1)+}$ and $\tau_{s,c}^{(1)-}$. These discrepancies will be caused by those effects that have different parity properties, i.e., the variation in sound speed and nonuniform magnetic field, both contribute to the flow maps. Although the effect of "uniform" mass flows in $\tau_{s,c}$ is much stronger than that of the magnetic field inhomogeneities, there must be a difference between the

TABLE 1

SYMMETRY PROPERTIES OF VARIOUS CONTRIBUTIONS TO THE PROPAGATION TIMES

Effect	Contribution to $\tau_{s,c}^{(1)}$	Contribution to $\tau_{s,c}^{(2)}$	Parity Property
Horizontal variation of sound speed	Yes	No	$\tau_{s,c}^{(1)+} = \tau_{s,c}^{(1)-}$
Uniform horizontal flow	Yes	No	$\tau_{s,c}^{(1)+} = -\tau_{s,c}^{(1)-}$
Variation in horizontal mass flow ($v_{\alpha\beta} \neq 0$)	No	Yes	$\tau_{s,c}^{(2)+} = -\tau_{s,c}^{(2)-}$
Uniform horizontal magnetic field	No	Yes	$\tau_{s,c}^{(2)+} = \tau_{s,c}^{(2)-}$
Variation in horizontal magnetic field ($b_{\alpha\beta} \neq 0$)	Yes	No	$\tau_{s,c}^{(1)+} = \tau_{s,c}^{(1)-}$
Uniform vertical flow	No	No	
Variation in vertical flow	Yes	No	$\tau_{s,c}^{(1)+} = -\tau_{s,c}^{(1)-}$
Variation in vertical magnetic field ($b_{z\alpha}$)	Yes	No	$\tau_{s,c}^{(1)+} = \tau_{s,c}^{(1)-}$

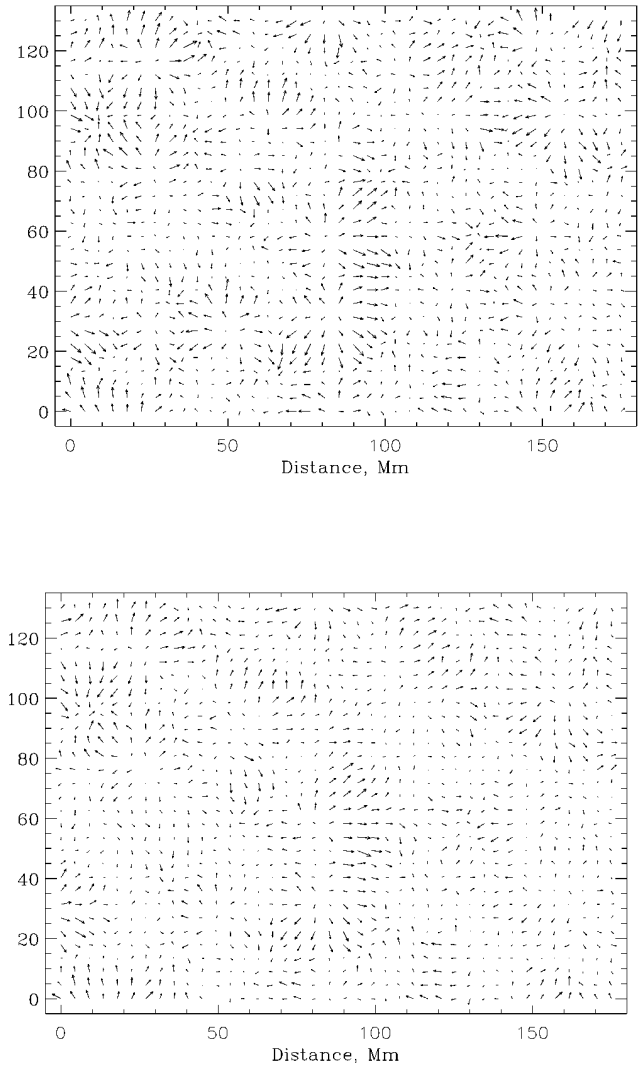

FIG. 3.—Reconstructed velocity field (*top*) at 1.2 Mm below the visible surface, $v_{max} = 2.3$ km s^{-1}, (*bottom*) at the depth of 2.8 Mm; $v_{max} = 1.76$ km s^{-1}.

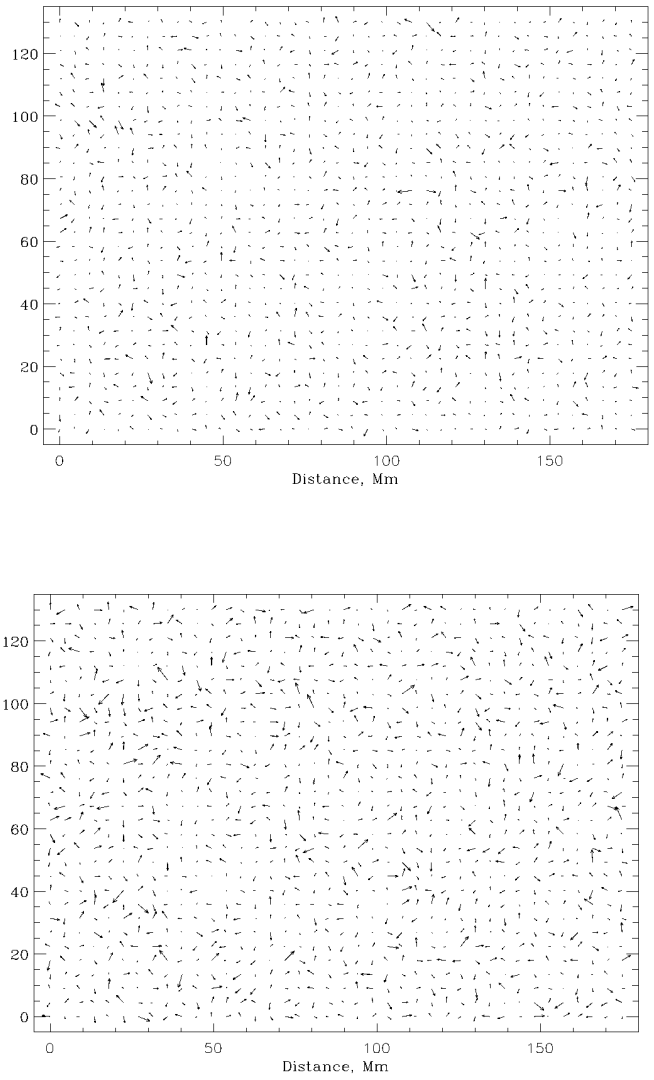

FIG. 4.—Discrepancies between the velocity maps obtained from forward and backward propagation times (*top*) at 1.2 Mm below the visible surface, (*bottom*) at 2.8 Mm.

velocity field reconstructed from the forward and backward propagation times. This difference should indicate the location of magnetic field inhomogeneities or/and variation in sound speed. As an example, we show in Figure 4 the map of velocity vectors that represent the difference between the velocities obtained from $\tau_{s,c}^{(1)+}$ and $\tau_{s,c}^{(1)-}$. One can see a clear correlation between the location of the largest discrepancies in the reconstructed velocity field and the locations of the strongest magnetic field both on the visible surface (Fig. 2*a*) and on the reconstructed magnetic field (v_A^2/c_s^2) at the same depth (Fig. 2*b*). To estimate the magnetic field strength we need to adopt some model parameters for plasma density below the surface. We try here the parameters given in the model of the convection zone by Spruit (1974): at the depth $h = 1.2$ Mm, $\rho = 0.3810^{-5}$ g cm^{-3}, which gives the estimate for sound speed $c_s = 14.8$ km s^{-1}; at $h = 2.8$ Mm, $\rho = 0.3610^{-4}$ g cm^{-3}, and $c_s = 18.4$ km s^{-1} (see also Hill 1995, and references therein). For these parameters at $h = 1.2$ Mm, the upper bound value of magnetic field strength is $B_{max} = 3480$ Gs; at $h = 2.8$ Mm, $B_{max} = 10{,}760$ Gs. Of course, these numbers are approximate; first of all the model parameters of convective zone need to be updated, and then, in the second harmonics of travel times only a contribution of magnetic field is taken into account while a possible influence of other factors is ignored. Figures 5*a* and 5*b* (Plate 11) show the maps for reconstructed magnetic field at $h = 1.2$ Mm and $h = 2.8$ Mm, respectively, (yellow color). One can see that at lower layers the flow pattern, which still mimics the supergranular picture, becomes weaker, and the magnetic field at lower layers becomes stronger and noticeably spread. The reason for this is that data used for these examples are averaged for several annuli, and the image of the magnetic field, as mentioned earlier, is required to be "homogeneous" over the space comparable with the radius of annuli where measurements were taken. Finally, the example of velocity field and the intensity of shear flows for both depths are shown in Figure 6 (Plate 12).

These preliminary results should be understood as an illustration of the way in which the proposed method can work. Note, however, that the velocity maps obtained here are very close to those obtained by Duvall et al. (1998). We are reminded that the flow maps shown in Figure 3 are computed using only forward propagation time (their first Fourier harmonics), while velocity maps in Duvall et al.

(1998) are obtained using the difference of forward and backward propagation times. As mentioned above, Fourier harmonics allow one to compute the velocity maps using either $\tau_{c,s}^{(1)+}$, or $\tau_{c,s}^{(1)-}$, or their half-difference $(\tau_{c,s}^{(1)+} - \tau_{c,s}^{(1)-})/2$. The data for the Fourier-transformed times and those used in four-quadrant approach were reduced in a different way (for Fourier harmonics the annulus was divided into eight segments, to preserve the accuracy the width of the segments was larger than in the case of four quadrants). The fact that all maps are very similar [the closest to flow field obtained from the four-quadrant method is naturally the one constructed with $(\tau_{c,s}^{(1)+} - \tau_{c,s}^{(1)-})/2$], is very encouraging. All these examples are still intermediate. With successfully operating MDI-*SOHO* and increasing the level of the accuracy of the data, we hope to include in our studies the influence of flow and magnetic field inhomogeneities at smaller scales and reconstruct the subsurface image for the arbitrary spatial dependence of flows and magnetic field possibly through the more of the convective zone.

6. DISCUSSION

We describe a new concept in time-distance analysis based on the idea that the different harmonics of Fourier transforms of the acoustic wave travel times measured as a function of direction give the information on the different physical properties of medium. The proposed method allows one to sort out in a regular way various characteristics of the subsurface medium, the flows, magnetic fields, and their nonuniformities. The method is less sensitive to the measurement errors and is designed as a regular method for future analysis; with the increasing resolution, higher harmonics will give the information about the smaller scale structures of subsurface layers. The inversion procedure will allow one to find the depth-dependent parameters.

The method suggests to use sin $n\theta$ and cos $n\theta$ transforms of the propagation time $\tau(\theta)$ measured between some point on the solar surface and points with the prescribed azimuthal angle θ around the annuli. It is shown that additional and rich information can be obtained from the analysis of parity properties (with respect to forward and backward propagation) of various contributions, including the spatial inhomogeneities of background parameters of medium; the parity properties of the contribution of mass flows, magnetic effects, and variation of sound speed with respect to forward and backward propagation, are different.

As an illustration of our method we discuss only the first two harmonics of Fourier sine and cosine transforms. It is shown for example that the first harmonic "average" ($n = 1$ in [2] and [3]) provides the information on the direction and speed of the horizontal plasma flows. The second harmonic "average" ($n = 2$ in [2] and [3]) allows one to find the orientation and absolute value of horizontal magnetic fields and the spatial gradients of flow velocity; namely, the sum of forward and backward propagating times, $\tau^{(+)} + \tau^{(-)}$, carries the information on the magnetic field distribution, while the difference, $\tau^{(+)} - \tau^{(-)}$, carries the information on the magnitude and orientation of shear flows. Remarkably, the vertical components of mass flow and magnetic field do not interfere with these measurements. Note that the accuracy of observational data at present does not allow one to find the values of shear by differentiating the calculated velocity field maps: one gets discontinuities wherever the velocity changes the sign, while in our approach some gradients of flow velocity can be directly found through the second harmonics of measured propagation times.

Using the Fourier-transformed times, one can construct the flow maps either from forward or from backward propagation times, or from they half-sum, $[\tau_{s,c}^{(1)+} + (-\tau_{s,c}^{(1)-})]/2$ (or half-difference of their absolute values); since the property $\tau_{s,c}^{(1)+} = -\tau_{s,c}^{(1)-}$ is valid only for strictly homogeneous flows, the "difference" map, i.e., the difference between the flow field obtained by $\tau_{s,c}^{(1)+}$ and $\tau_{s,c}^{(1)-}$ shows the regions where the inhomogeneities are distributed and their strength. This information may be used as an additional test.

The advantage of sin $n\theta$ and cos $n\theta$ transforms, besides the possibility of obtaining the information about magnetic fields, the velocity gradients, etc., is in its intrinsic invariance with respect to the choice of the coordinate frame. The method provides an automatic rule of assigning proper weights to every observation point and allows one to sort out the effects of magnetic field, flows, and their inhomogeneities in a unified way. Its efficiency is especially useful in the problem of the flow maps for annular distances comparable with the size of the supergranular convection. The point is that with increasing the annulus there occurs a reduction of the local velocity: as soon as the annulus size becomes comparable to the size of the chosen convection cells, a partial cancellation of the oppositely directed velocities occurs. We have computed the errors in reconstruction of the flow field as a function of annular radii and have shown how sin $n\theta$, cos $n\theta$ transforms "kill" the largest source of errors in the prediction of velocity fields.

As a mere illustration we apply our approach to the concrete set of observational data obtained from the MDI-*SOHO* instrument. The data were reduced by T. L. Duvall. Of course, the results obtained for given observational data (of January 27) should be understood as the imaging of a "large-scale" horizontal structure of magnetic field and mass flows, e.g., their variation over the space comparable with the radiis of annuli where the measurements are taken. This method, however, allows to consider the case when background parameters weakly (linearly) depend on the horizontal coordinates and thus to find a variation of shear flows using the difference between the second harmonics of the forward and backward propagation times. Even these preliminary results clearly show the flow pattern corresponding to supergranular flows. The flow maps are close to those obtained in Duvall et al. (1998), which support both approaches. In addition, through the "difference" map we obtained the maps for the distribution of the strongest inhomogeneities. These maps are well correlated with the magnetic field pattern both on the surface (the observed magnetogram) and the reconstructed field below the surface. Although several physical parameters contribute to the map of inhomogeneities, this correlation seems natural, because the presence of magnetic field implies the distortion in sound speed, horizontal and vertical flows, etc.

Note that another limitation on the use of our technique stems from our tacit assumption that the terms of order u^2/c_s^2 can be neglected. These terms also give a contribution to the $\tau_s^{(2)}$ and $\tau_c^{(2)}$, and can be mixed up with magnetic terms. Clearly, they are small compared to the latter if u is less than v_A. If the opposite is valid, then evaluation of the magnetic field becomes difficult. But the general trend of the dominance of the flow in the first harmonic "average" and the magnetic field in the second harmonic "average"

should persist. The influence of strong inhomogeneities with the scale much less than the radius of the annulus requires the special approach. The study of this more general case is under way.

MDI-*SOHO* data used here were reduced by Tom Duvall. Tom Duvall also made sine and cosine transforms of measured travel times, and we thank him for his great work. We thank Ted Tarbell for many helpful comments. We are grateful to the referee for extremely detailed analysis of the paper and many valuable suggestions. M. R. is grateful to Jave Kane for providing computing support. This work is supported by NASA grant NAG5-3077 at Stanford University.

APPENDIX A

EFFECTS OF DISCRETE MESH

In the actual data analysis with the discrete points over the annulus we have to take a sum instead of the integral (eq. [1]). The important factor in this analysis is that the discreteness of data cause the error that, in principle, can be minimized.

The generalization of our results to the case of a finite number of grid points is straightforward. One should replace the integral forms (eqs. [2] and [3]) by their discrete analogue

$$\bar{\tau}_c^{(n)} = \frac{1}{N} \sum_{i=1}^{N} \tau_i(\theta_i) \cos n\theta_i \tag{A1}$$

$$\bar{\tau}_s^{(n)} = \frac{1}{N} \sum_{i=1}^{N} \tau_i(\theta_i) \sin n\theta_i \,, \tag{A2}$$

where θ_i stands for a polar angle of the ith grid point within the annulus. Let $N = 2k$ be the number of points at circle. Denote the angle $\theta_k = 2\pi k/N$ with $k = 0, 1, 2, 3, \ldots, N-1$. let the flow velocity has a direction θ_u. "Correct" distribution of propagation times is

$$\tau_k = \tau_0 + \Delta\tau \cos(\theta_k - \theta_u) \,. \tag{A3}$$

Assume that the measured values of τ have small errors, $\Delta\tau_k$, i.e., the measured values of τ_k are

$$\tau_k = \tau_0 + \Delta\tau \cos(\theta_k - \theta_u) + \Delta\tau_k \,. \tag{A4}$$

Using equation (A4) as input data for equations (A1) and (A2), we can find what the values of θ_u, u, θ_B, and B will be.

We find it important to discuss some problems that may appear in analyzing the observational results with a "coarse" grid, when only a few points are situated within the annulus and/or they are distributed unevenly. In this case, even in the absence of mass flows and magnetic field one could find nonzero values of $\tau_s^{(n)}$ and $\tau_c^{(n)}$. To avoid these kinds of errors one could first subtract the average value of τ from the measurements and only then do relationships (A1) and (A2) apply. After that one could apply a further "smoothing" procedure by making all calculations in a set of frames turned with respect to the initial one by a sequence of slightly different angles,

$$\theta_k = \frac{k}{N} 2\pi \,, \qquad k = 0, 1, \ldots, N-1 \,. \tag{A5}$$

This problem will not arise if the grid points, though distributed unevenly over the azimuth of the annulus, are distributed so that they are symmetric with respect to the axes $0x$ and $0y$. A different kind of problem may arise, though, if the grid points are situated at different radial distances from a center of annulus. In this case the correction to the unperturbed propagation time may be introduced.

APPENDIX B

"MAGNETIC" CORRECTIONS TO THE PROPAGATION TIME IN A VERTICALLY STRATIFIED ATMOSPHERE

In this appendix we generalize the method to the case of a vertically stratified atmosphere, and derive the equations of § 3 with depth-dependent sound speed $c_s(z)$. In fact, in our previous analysis sound speed also depended on z but in a stepwise manner, so that the ray did not penetrate into the hotter slab and remained within the slab of uniform velocity.

We start with the expression for the correction to the propagation time

$$\delta\tau = -\int_S \frac{ds}{v_{\rm gr}} \frac{\delta v_g}{v_g} \,, \tag{B1}$$

where integration is carried out along the unperturbed ray trajectory. In our case, $v_g = c_s$, $\delta v_{gr} = (v_A^2/2c_s)[1 - (\boldsymbol{nb})^2]$ (see eq. [8]). By noting that $ds/v_g = dv_z/v_{gz}$, where v_{gz} is the vertical component of the group velocity, one finds that

$$\delta\tau = -2\int_0^h \frac{dz}{v_{gz}}\frac{\delta v_g}{v_g} = -\int_0^h \frac{v_A^2[1-(\boldsymbol{nb})^2]dz}{c_s^3 n_z} . \tag{B2}$$

As earlier, h is the depth of the layer where reflection of the ray occurs ($k_z = 0$). The factor "2" in the first of equality of [B2]) takes into account two branches of the ray trajectory, descending and ascending. From the condition $\omega = \text{const}$ we have

$$c_s^2(h)(k_x^2 + k_y^2) = c_s^2(z)(k_x^2 + k_y^2 + k_z^2) . \tag{B3}$$

In the system where x and y are ignorable coordinates, k_x and k_y are conserved quantities. We have therefore,

$$k_z = \sqrt{k_x^2 + k_y^2}\sqrt{1 - \frac{c_s^2(z)}{c_s^2(h)}} \tag{B4}$$

and

$$n_z = \sqrt{1 - \frac{c_s^2(z)}{c_s^2(h)}} ; \qquad n_x = \frac{c_s(z)}{c_s(h)}\cos\theta ; \qquad n_y = \frac{c_s(z)}{c_s(h)}\sin\theta . \tag{B5}$$

We will take into account both vertical variation of the Alfvén velocity [$v_A = v_A(z)$] and the direction of the horizontal magnetic field, $\theta_B = \theta_B(z)$. We have

$$(\boldsymbol{nb})^2 = \cos^2(\theta - \theta_B)\frac{c_s^2(z)}{c_s^2(h)} \tag{B6}$$

Taking into account relations (B2), (B5), and (B6) we find

$$\delta\tau = -\int_0^h \frac{v_A^2(z)c_s^2(h)[1 - \cos^2(\theta - \theta_B(z)]}{c_s^4(z)\sqrt{c_s^2(h) - c_s^2(z)}}\, dz \tag{B7}$$

or

$$\delta\tau = -\int_0^h \frac{v_A^2(z)c_s^2(h)[1 - \cos 2\theta\cos 2\theta_B(z) - \sin 2\theta\sin 2\theta_B(z)]}{c_s^4(z)\sqrt{c_s^2(h) - c_s^2(z)}}\, dz . \tag{B8}$$

Remarkably, in this much more general case $\delta\tau$ still manifests the same $\cos 2\theta$, $\sin 2\theta$ dependence on the azimuthal angle as in the model of a uniform slab. Recall that in the case of a uniform slab $(\boldsymbol{nb})^2 = (r^2/r^+4h^2)\cos^2(\theta - \theta_B)$, $n_z = 2h/(r^+4h^2)^{1/2}$, and one recovers equation (21). For cosine and sine transforms now instead of equations (22) and (23) we have

$$\tau_s^{(2)} = \frac{1}{4}\int_0^h \frac{v_A^2(z)c_s^2(h)\sin 2\theta_B(z)}{c_s^4(z)\sqrt{c_s^2(h) - c_s^2(z)}}\, dz \tag{B9}$$

and

$$\tau_c^{(2)} = \frac{1}{4}\int_0^h \frac{v_A^2(z)c_s^2(h)\cos 2\theta_B(z)}{c_s^4(z)\sqrt{c_s^2(h) - c_s^2(z)}}\, dz . \tag{B10}$$

Probing different annuli, in other words, different reflection depths, and using a standard inversion procedure, one can find by virtue of equations (21) and (22) the distribution of the horizontal magnetic field and its depth dependence.

It is also important that for known $c_s(z)$ one can apply Abel inversion $\tau_s^{(2)}$ and $\tau_c^{(2)}$ and obtain in this way both magnitude and direction of the horizontal magnetic field. We leave a detailed analysis of this problem to future publication.

APPENDIX C

THE TRAVEL-TIME PERTURBATIONS OVER ANNULAR DISTANCES COMPARABLE WITH THE SCALE OF CONVECTION

We address here the problem of the accuracy of reconstruction of subsurface flows over annular distances that become close to the scale of convective motions (granular, mezogranular, supergranular).

As has already been mentioned in the main body of the paper, one can expect a reasonable accuracy of the reconstruction of the velocity field for the annuli of the radius that is small compared to the characteristic scale of the supergranular convection. In this appendix we present a more quantitative analysis of the problem for a particular model of convective motions and find the expression for time perturbation as a function of annular distances. Our analysis will also shed some light on the role of vertical motions.

We assume the model velocity field of the form:

$$v_x = \frac{v_0}{2} \sin qx \cos qy\,, \qquad v_y = \frac{v_0}{2} \cos qx \sin qy\,, \qquad v_z = -v_0 \cos qx \cos qy\,. \tag{C1}$$

This is one of the possible symmetries of the convection pattern having a square convective cells; obviously the model can be extended to hexagonal symmetry as well.

The origin of the coordinate frame is taken situated on the solar surface. The divergence of this velocity field is zero. The fluid experiences upwelling near the points $x = 0$, $y = 0$, $x = \pi/q$, $y = \pi/q$, etc., and downdraft near the points $x = 0$, $y = \pi/q$, $x = \pi/q$, $y = 0$, etc. Of course, the linear dependence of the vertical velocity on z can be assumed to be not very far from the solar surface, but this is exactly the area we are interested in.

Let the center of the annulus be situated in some point x_0, y_0. Then the ray trajectory can be presented in the following parametric form:

$$x = x_0 + \frac{t}{\tau} r \cos(\theta - \theta_0)\,, \tag{C2}$$

$$y = y_0 + \frac{t}{\tau} r \sin(\theta - \theta_0)\,, \tag{C3}$$

$$z = -h \frac{2t}{\tau}\,, \qquad 0 < t < \frac{\tau}{2}\,,$$

$$z = 2h\left(1 - \frac{t}{\tau}\right), \qquad \frac{\tau}{2} < t < \tau\,, \tag{C4}$$

where time is counted from $t = 0$ to $t = \tau$ (the total propagation time in the absence of flows is $\tau = (r^2 + 4h^2)^{1/2}/c_s$). Angle θ_0 represents the a priori unknown orientation of the convective motion with respect to the observation mesh. The correction $\delta\tau(\theta)$ to the propagation time associated with the presence of the flows is

$$\delta\tau = \int_0^\tau \frac{\boldsymbol{un}}{c_s}\, dt\,, \tag{C5}$$

where integration is carried out along the ray trajectory (C2)–(C4), and where $\boldsymbol{n}$ is a unit vector along the ray trajectory,

$$n_x = \frac{r \cos\bar\theta}{\sqrt{r^2 + 4h^2}}\,, \qquad n_y = \frac{r \sin\bar\theta}{\sqrt{r^2 + 4h^2}}\,, \qquad n_z = \pm\frac{2h}{\sqrt{r^2 + 4h^2}}\,. \tag{C6}$$

We introduced here a notation $\bar\theta = \theta - \theta_0$; the upper and the lower signs correspond to the descending and ascending branches of the trajectory, respectively. We have

$$\delta\tau = \frac{v_0}{2c_s\sqrt{r^2 + 4h^2}} \left\{ r \int_0^\tau [\cos\bar\theta \sin qx \cos qy + \sin\bar\theta \cos qx \sin qy] \right.$$
$$\left. + qh^2 \left[\int_0^{\tau/2} \frac{t}{\tau} \cos qx \cos qy\, dt - \int_{\tau/2}^\tau 1 - \frac{t}{\tau} \cos qx \cos qy\, dt \right] \right\}. \tag{C7}$$

Instead of carrying out exact integrations (which is possible), we find several terms in the expansion over the powers of r and h (in the present time-distance analysis $r \simeq 3h$; Duvall 1982). To do this, one can use the identities of the type

$$\sin\left(qx_0 + qr\frac{t}{\tau}\cos\bar\theta\right)\cos\left(qy_0 + qr\frac{t}{\tau}\sin\bar\theta\right)$$
$$= \sin qx_0 \cos qy_0 \cos\left(qr\frac{t}{\tau}\cos\bar\theta\right)\cos\left(qr\frac{t}{\tau}\sin\bar\theta\right)$$
$$+ \cos qx_0 \cos qy_0 \sin\left(qr\frac{t}{\tau}\cos\bar\theta\right)\cos\left(qr\frac{t}{\tau}\sin\bar\theta\right)$$
$$- \sin qx_0 \sin qy_0 \cos\left(qr\frac{t}{\tau}\cos\bar\theta\right)\sin\left(qr\frac{t}{\tau}\sin\bar\theta\right)$$
$$- \cos qx_0 \sin qy_0 \sin\left(qr\frac{t}{\tau}\cos\bar\theta\right)\sin\left(qr\frac{t}{\tau}\sin\bar\theta\right). \tag{C8}$$

If we make r equal to zero, then in the above expression only the first term survives. This term corresponds to the model of a uniform flow, with u independent of x and y. This case is studied in § 3. Retaining the terms up to the second order in qr, we

obtain

$$\sin\left(qx_0 + qr\cos\bar{\theta}\,\frac{t}{\tau}\right)\cos\left(qy_0 + qr\sin\bar{\theta}\,\frac{t}{\tau}\right)$$
$$\simeq \sin qx_0 \sin qy_0 - \frac{t^2}{2\tau^2}(qr)^2 \sin qx_0 \cos qy_0$$
$$+ qr\,\frac{t}{\tau}\cos\bar{\theta}\cos qx_0\cos qy_0 - qr\,\frac{t}{\tau}\sin\bar{\theta}\sin qx_0\sin qy_0$$
$$- \frac{t^2}{\tau^2}(qr)^2\cos qx_0\sin qy_0\cos\bar{\theta}\sin\bar{\theta}\,. \tag{C9}$$

In this fashion one obtains from (C7) corrections to the perturbation of travel time:

$$\delta\tau = \frac{v_0 r\tau}{2c_s\sqrt{r^2+4h^2}}$$
$$\times\left\{(\cos\bar{\theta}\sin qx_0\cos qy_0 + \sin\bar{\theta}\cos qx_0\sin qy_0)\left(1 - \frac{q^2r^2}{4} - \frac{2q^2h^2}{3}\right)\right.$$
$$+ \frac{qr}{2}(\cos qx_0\cos qy_0 - \sin 2\bar{\theta}\sin qx_0\sin qy_0)$$
$$\left.+ \frac{q^2r^2}{6}(\sin qx_0\cos qy_0\cos 3\bar{\theta} - \cos qx_0\sin qy_0\sin 3\bar{\theta})\right\}. \tag{C10}$$

At $qr \to 0$, $qh \to 0$, this expression coincides with equation (14) for the model of a uniform flow. At larger annuli, when qr and qh are finite, there appear additional terms, which cause an error in the prediction of velocity field. It is important that the sin $n\theta$, cos $n\theta$ transforms "kills" the largest source of errors, the linear term that is proportional to qr, as well as the terms containing higher harmonics. These calculation clearly show the advantage of Fourier transforms of travel time.

The other observation that can be made from the expression (C10) is that nonuniform vertical flows contribute only to the second-order corrections (to the term proportional to q^2r^2).

When the second-order corrections (found by Fourier transform method) are retained, the change in the local velocity is described by the factor of the first term in the right-hand side of equation (C10); using the rough relationship $r \simeq 3h$, we get for this factor an estimate

$$1 - \frac{q^2r^2}{4} - \frac{2q^2h^2}{3} \simeq 1 - \frac{1}{3}q^2r^2\,. \tag{C11}$$

This shows that when increasing the annulus an apparent reduction of the local velocity occurs. This general trend is quite clear: as soon as the annulus size becomes comparable with the size of the chosen convection cells, a partial cancellation of the oppositely directed velocities occurs. It is important that if the Fourier transform is used then the prediction with regard to the direction of the velocity is less sensitive to the parameter qr: the angular dependence of the first term in (C10) does not change compared to the case of $r \to 0$, $h \to 0$.

REFERENCES

Bogdan, T. J. 1995, in ESA 4th *SOHO* Workshop, Helioseismology, ed. J. T. Hoeksema, et al. (Noordwijk: ESA), 31
Braun, D. C., Duvall, T. L., Jr., & LaBonte, B. J. 1987, ApJ, 319, L27
Braun, D. C., Duvall, T. L., Jr., & LaBonte, B. J. 1988, 335, 1015
Braun, D. C., Duvall, T. L., Jr., LaBonte, B. J., Jefferies, S. M., Harvey, J. W., & Pomerantz, M. A. 1992, ApJ, 391, L113
Braun, D. C., LaBonte, B. J., & Duvall, T. L., Jr. 1990, ApJ, 354, 372
Duvall, T. L., Jr. 1982, Nature, 300, 242
Duvall, T. L., Jr., D'Silva, S., Jefferies, S. M., Harvey, J. W., & Schou, J. 1996, Nature, 379, 235
Duvall, T. L., Jr., Jefferies, S. M., Harvey, J. W., & Pomerantz, M. A. 1993, Nature, 362, 430
Duvall, T. L., Jr., et al. 1998, Sol. Phys., submitted
Hill, F. 1995, in ESA 4th *SOHO* Workshop, Helioseismology, ed. J. T. Hoeksema, et al. (Noordwijk: ESA), 63
Hindman, B. W., Zweibel, E. G., & Cally, P. S. 1996, ApJ, 459, 760
LaBonte, B J., & Ryutova, M. P. 1993, ApJ, 419, 388
Ryutova, M., Kaisig, M., & Tajima, T. 1991, ApJ, 380, 268
Ryutova, M., & Persson, M. 1984, Phys. Scr., 29, 353
Ryutova, M. P., & Priest, E. R. 1993a, ApJ, 419, 349
———. 1993b, ApJ, 419, 371
Spruit, H. C. 1974, Sol. Phys., 34, 277

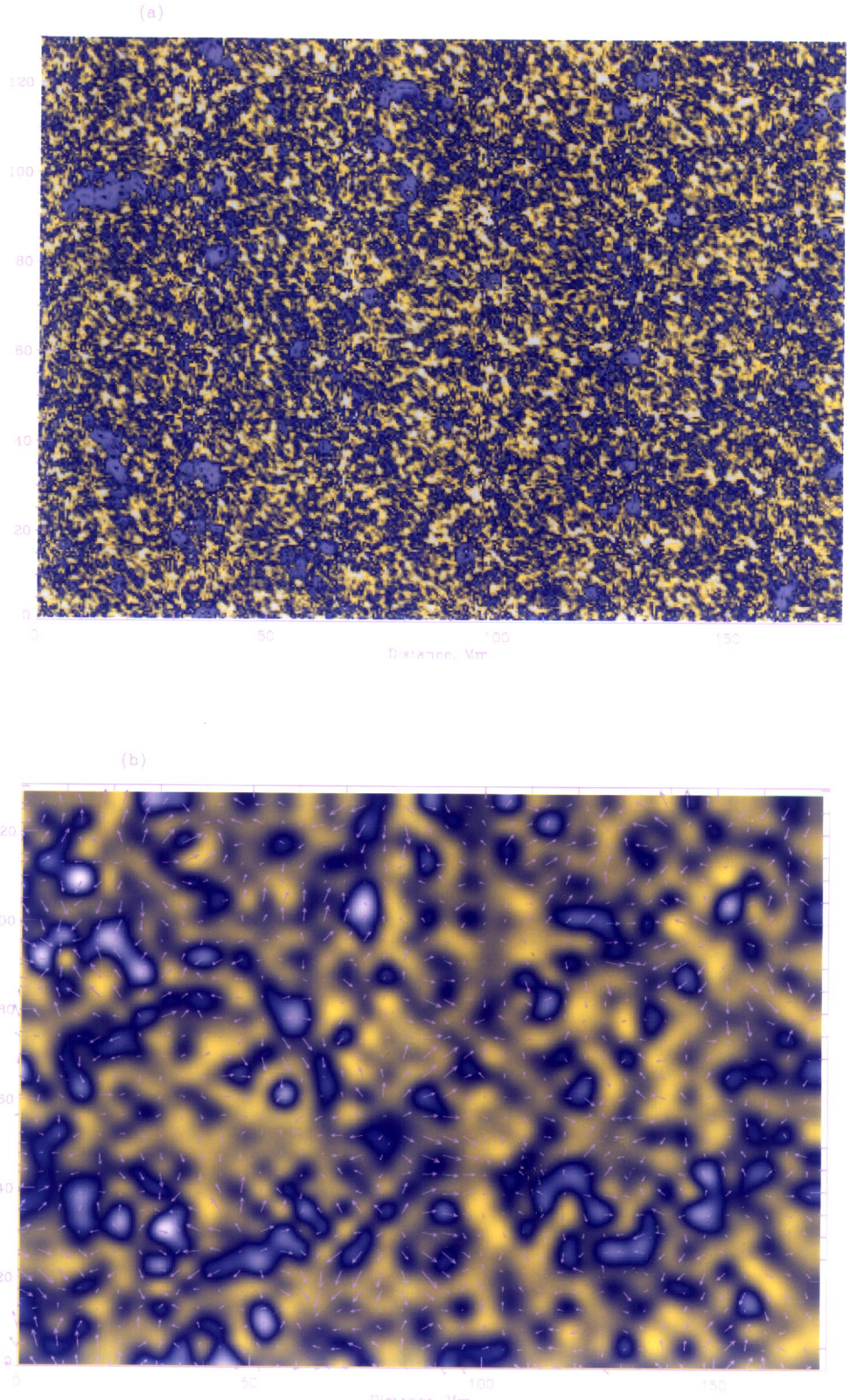

FIG. 2.—*Top*: MDI high-resolution magnetogram of the studied region, 1996 January 27. *Bottom*: Distribution of the horizontal magnetic field in terms of inverse plasma beta, v_A^2/c_s^2 at 1.2 Mm below the visible surface, $(v_A^2/c_s^2)_{max} = 0.11$.

RYUTOVA & SCHERRER (see 494, 443)

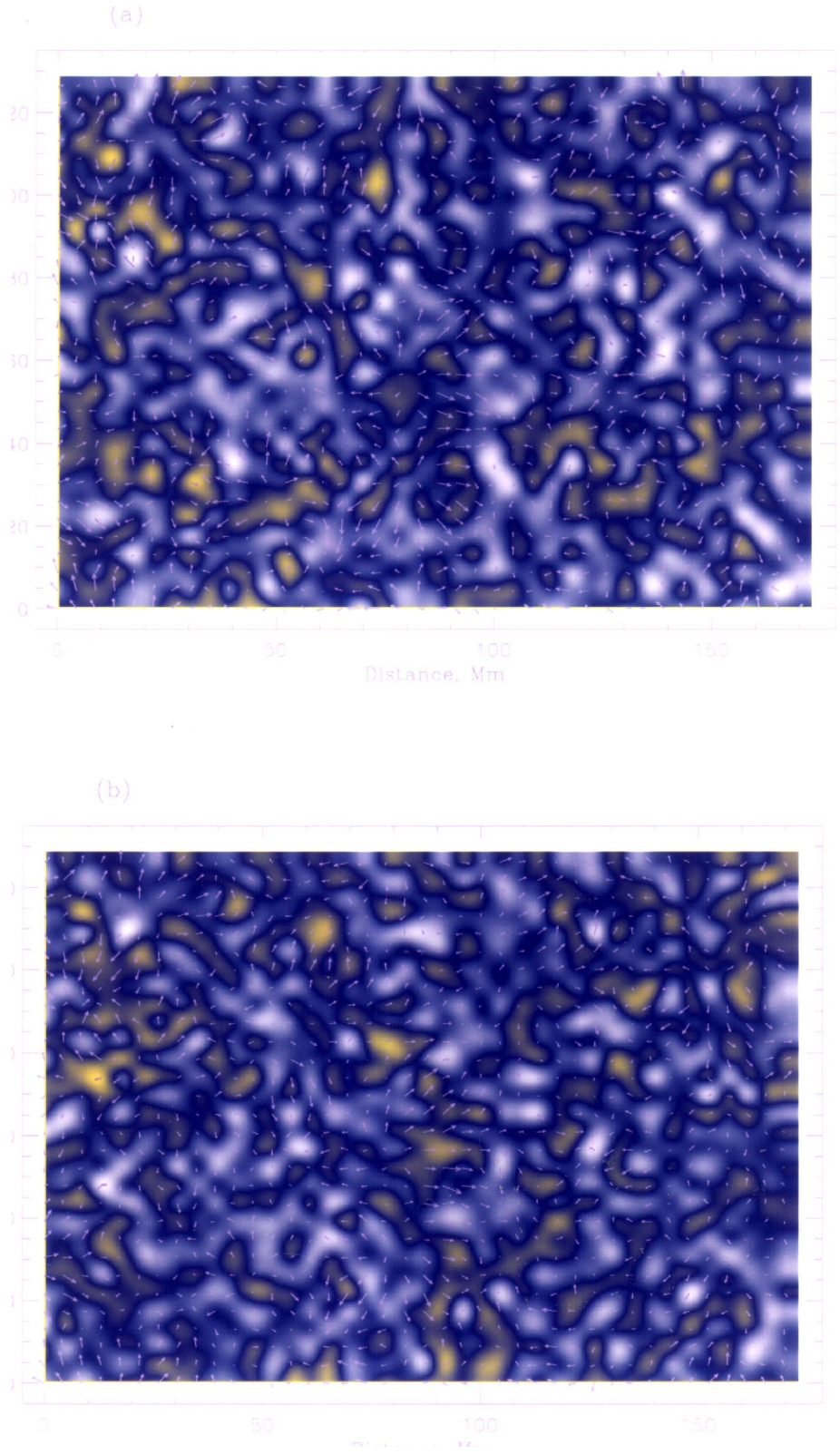

FIG. 5.—Magnetic and velocity fields (*top*) at 1.2 Mm below the visible surface, $B_{max} \simeq 3480$ Gs, (*bottom*) at 2.8 Mm below the surface; $B_{max} \simeq 10{,}760$ Gs

RYUTOVA & SCHERRER (see 494, 444)

PLATE 11

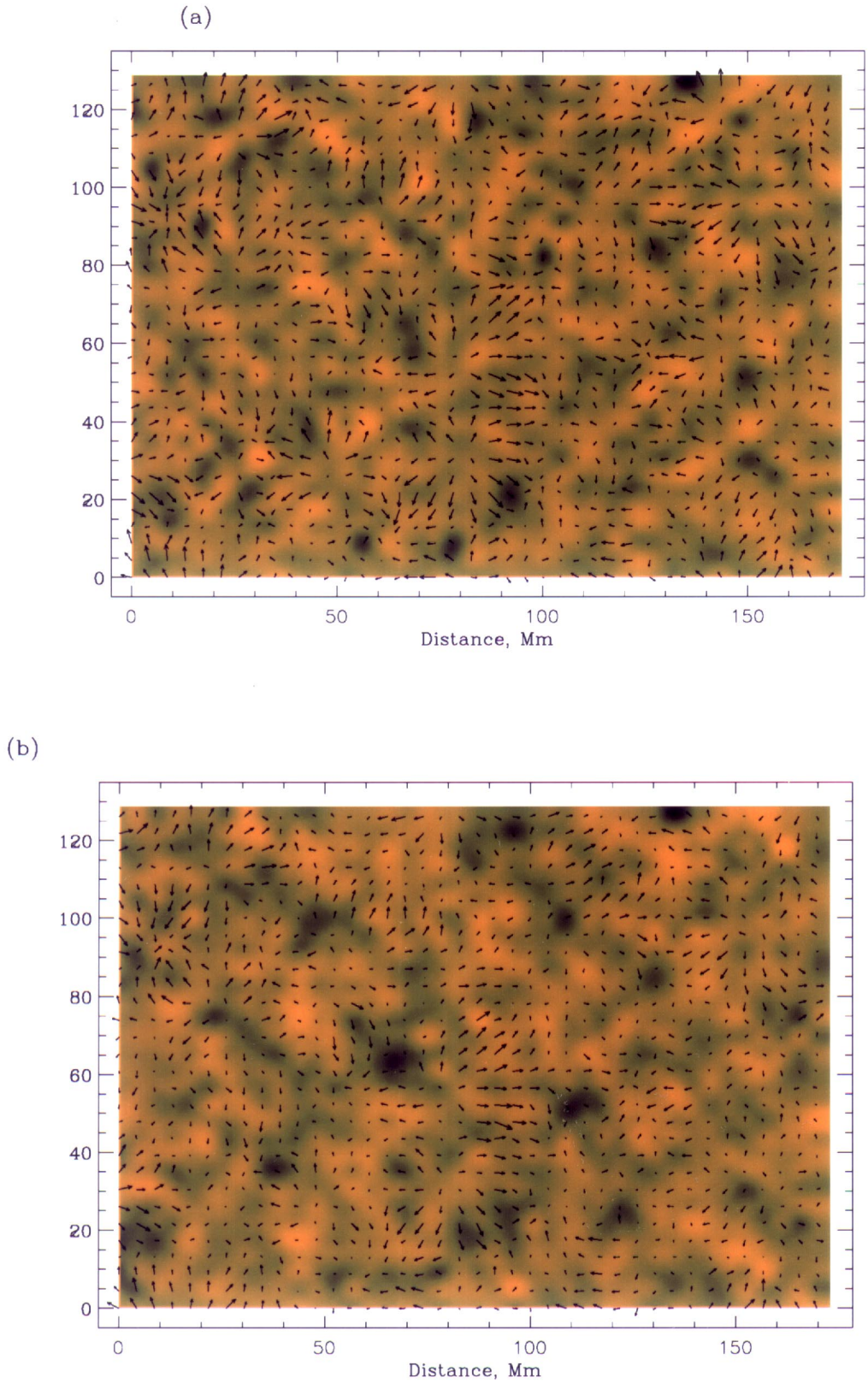

FIG. 6.—Velocity field and the velocity shear $D_{Hz} = \partial u_x/\partial x - \partial u_y/\partial y$ (*a*) at the depth 1.2 Mm, $D_{Hz,max} \simeq 0.67 \times 10^{-3}$ s^{-1}, (*b*) at 2.8 Mm, $D_{Hz,max} \simeq 0.29 \times 10^{-3}$ s^{-1}.

RYUTOVA & SCHERRER (see 494, 444)

PLATE 12